

# Holographic Radius Test Plates

Quandou Wang, Johannes A. Soons, and Ulf Griesmann

National Institute of Standards and Technology (NIST), Physical Measurement Laboratory,  
Semiconductor & Dimensional Metrology Division, Gaithersburg, MD 20899-8223, USA

## ABSTRACT

We evaluate a method for testing the radius of a spherical surface with a hologram that consists of a pair of nested Fresnel zone lenses. The hologram is positioned in the collimated test beam of a Fizeau interferometer. The inner zone lens generates a focus at the test part surface, whereas the wavefront of the first diffraction order of the outer zone lens is confocal with the test part. When the test part radius is equal to the nominal radius, the fringes in both zone lens areas are nulled at the same distance of the test sphere from the zone lens. The radius error of the spherical surface can be calculated from the test sphere displacement between interferometer null positions for the inner and outer zone lenses, or from the defocus term of the outer (confocal) lens at the position of zero defocus of the inner (cat's-eye) zone lens. The primary benefits of the nested zone lens method are its ease of use, and that it enables radius measurements of spherical surfaces with large radii. We describe the radius measurement of a precise convex sphere with a nominal radius of 80 mm.

**Keywords:** Optical interferometry, Radius test plates, Computer-generated hologram

## 1. INTRODUCTION

Radius test plates are widely used for the inspection of spherical optical lens surfaces during lens fabrication.<sup>1</sup> The test plates are precision spherical surfaces with known radius that are brought into contact with a spherical test surface. The Newton fringes that are observed when the surface pair is illuminated with coherent light can be used to infer the difference in radius between the test plate and the spherical test surface. The greatest advantage of radius test plates is their ease of use, which, in many cases, outweighs the disadvantages that optics fabricators must maintain a large set of concave and convex test plates and that the visual inspection of Newton fringes results in a relatively large uncertainty in the radius estimation. Much lower measurement uncertainty for the radii of convex and concave spherical surfaces can be achieved with the interferometric radius bench method.<sup>2,3</sup> This method combines a phase-shifting interferometer,<sup>4</sup> that is equipped with a Fizeau objective (transmission sphere), with metrology for measuring the displacement of the test part along the optical axis. The part is moved from the “confocal” position, at which the test part center is at the focus of the spherical test wavefront, to the “cat's-eye” position, at which the test wavefront focus is on the test part surface. The displacement between the two positions is the test part radius. When the test part position is tracked with a displacement measuring laser interferometer, relative uncertainties of  $10^{-4}$  or below can be achieved.<sup>2,3,5,6</sup> The obvious disadvantage of an interferometric radius bench is that it requires expensive equipment and highly trained operators.

In this paper we explore an alternative method for testing and measuring the radius of a spherical test surface, which uses a nested Fresnel zone lens pair to generate two spherical test wavefronts that separately define the confocal and cat's-eye test positions.<sup>7</sup> The nested zone lens also makes it possible to integrate the displacement metrology into the zone lens itself. A holographic test plate can be used to measure small deviations in the radius of a spherical test surface from a known nominal radius. The zone lens uses a nested design whose inner zone lens, in first diffraction order, creates a focus on the test sphere surface. In other words, the inner zone lens sets the distance between the nested zone lens and the test part, and, in principle, can be used to measure small displacements around the cat's-eye position. The outer zone lens is designed to have a focus at the center of the test sphere when the focus of the inner zone lens is on the test sphere surface. The defocus of the outer zone provides an estimate for the displacement of the sphere relative to this position, which equals the radius error. We demonstrate the method with a measurement of the radius of a precise reference sphere that has a nominal radius of 80 mm, and describe the sources of measurement uncertainty.

---

Author contact emails: [quandou.wang@nist.gov](mailto:quandou.wang@nist.gov), [johannes.soons@nist.gov](mailto:johannes.soons@nist.gov), [ulf.griesmann@nist.gov](mailto:ulf.griesmann@nist.gov)

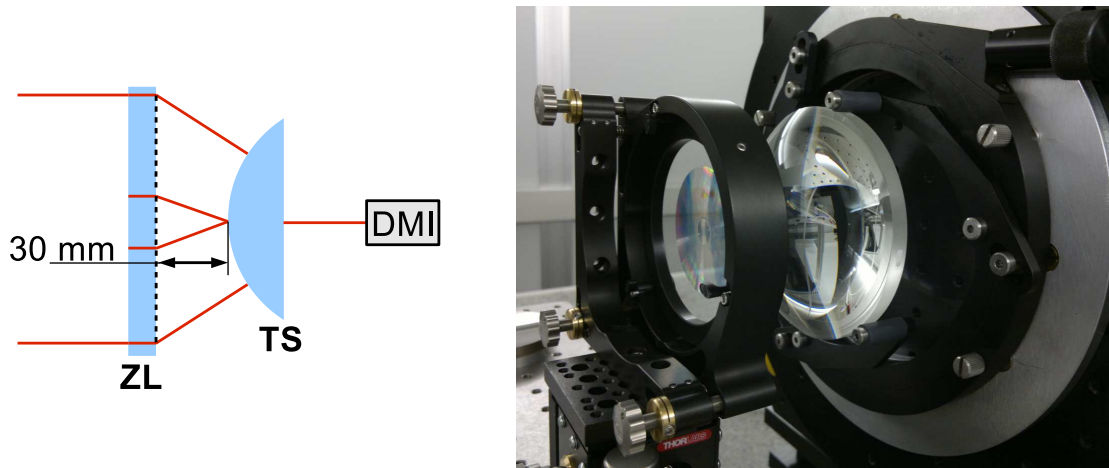


Figure 1. Setup for the radius measurement of a precise test sphere (TS) with 80 mm radius using a nested zone lens (ZL). A displacement-measuring laser interferometer (DMI) tracked the movement of the test part along the optical axis. A sketch of the setup is shown on the left, a photograph of the actual setup on the right.

## 2. MEASUREMENT SETUP AND ZONE LENS FABRICATION

The concept of our measurement is illustrated in Fig. 1 (left side). We designed a zone lens to test a very precise reference sphere that has a nominal radius of 80 mm. It has a reported radius of  $(79988.169 \pm 0.04) \mu\text{m}$  ( $k=2$ ). The measurement setup was modeled with commercial optical modeling software for a distance between zone lens and test sphere of 30 mm, as shown in Fig. 1. The inner zone lens was designed with a diameter of 12 mm; the outer zone lens has a 60 mm diameter. The phase functions of the central and outer zone lenses were obtained with the optical modeling software. Both zone lenses were described as even-order radial polynomials with terms up to the 8<sup>th</sup> order. The phase function was converted into a binary layout for the zone lenses suitable for lithographic fabrication of the lenses (shown in Fig. 2).

In our measurements, the interferometer cavity is formed by the back surface of the zone lens substrate, which becomes the reference surface of the interferometer, and the spherical test surface. The zone lens itself was fabricated to have very low diffraction efficiency in the 0<sup>th</sup> diffraction order.<sup>8</sup> Phase-shifting measurements were made by mechanically shifting the test part in the direction of the optical axis with a piezo-electric phase shifter that is integrated into the test part mount. A phase-shifting algorithm with 7 samples and 90° phase steps was used.<sup>9</sup> During our measurements we tracked the movement of the test sphere with a displacement-measuring laser interferometer (DMI).

The nested zone lens was fabricated at the National Institute of Standards and Technology (NIST). A plane-parallel substrate with 100 mm diameter and 6.5 mm thickness, made from a borosilicate float glass, was coated with an approximately 600 nm thick layer of photoresist. The nested zone lens layout, which is shown on the left of Fig. 2, was then written into the photoresist using the Zone Plate Array Lithography (ZPAL) tool<sup>10,11</sup> at NIST. After developing the photoresist, the zone lens patterns were etched to a depth of about 540 nm<sup>12</sup> using reactive ion etching. Finally, the photoresist layer was removed. A finished test plate, installed in the interferometer with the test sphere, is shown in Fig. 1. The fringes shown on the right side of Fig. 2 are observed when the distance between the nested zone lens and the test sphere is close to the design distance of 30 mm. Good fringe contrast was obtained for both the inner and the outer zone lenses. The mottling that is visible in the fringe image of Fig. 2 is due to a mid-spatial frequency flatness error in the inexpensive substrates. The astigmatism that is also visible in the fringe image is due to a flatness error of the substrate.

## 3. MEASUREMENT RESULTS AND DISCUSSION

After aligning the nested zone lens and the test sphere in the collimated test beam of the “eXtremely accurate CALibration InterferometerR” (XCALIBIR) at NIST, as shown in Fig. 1, the sphere was positioned close to the focus of the inner zone lens. The right side of Fig. 2 shows the fringes that were observed in the inner and outer zone lens areas. Several phase measurements were made with the test sphere positioned on either side of the inner zone lens focus (null), as is shown in Fig. 3. The relative displacement between measurement positions along the optical axis was measured with a

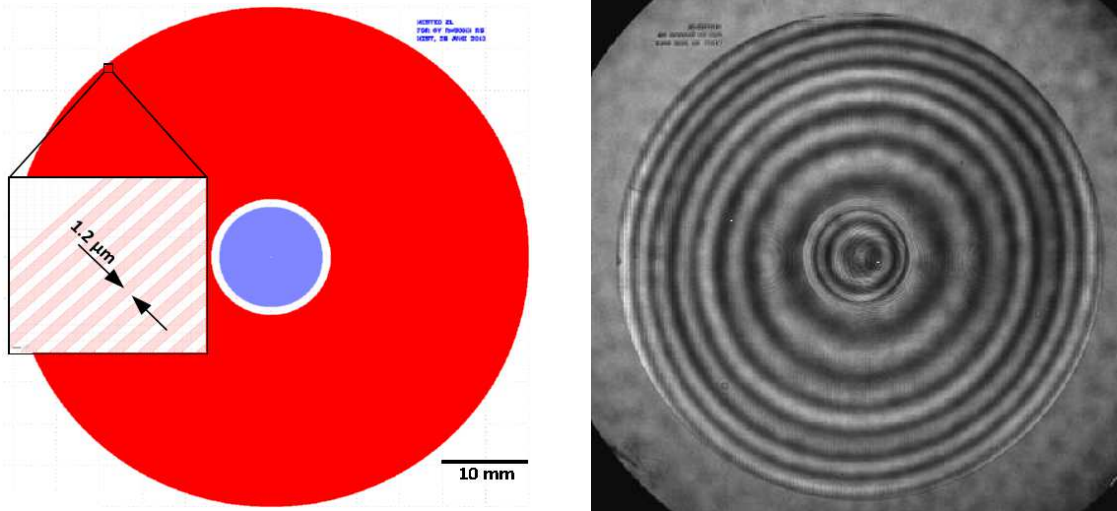


Figure 2. Layout of the nested zone lens (left) and interferogram obtained with the measurement setup shown in Fig. 1 (right). The inner zone lens has a diameter of 12 mm, the outer zone lens a diameter of 60 mm.

displacement measuring laser interferometer (DMI) having an effective Abbe offset of less than 1 mm (see Fig. 1). Five phase measurements were made at each position. Fig. 3 summarizes the results of these measurements. It shows the Zernike coefficient  $a_2^0$  (power)<sup>13</sup> for the inner and outer zone lenses for each of the five measurements that were made at all positions of the test sphere. On the scale of Fig. 3, the variability of the individual measurements cannot be discerned. The solid curves through the experimental data in Fig. 3 are parabolas to account for the non-linear dependence of the power term  $a_2^0$  on the displacement. The non-linearity is small but significant, in particular for the inner zone lens. Its cause is the inherently non-linear relation between power and displacement<sup>14</sup> and the radial shear of wavefronts in the inner and outer zone lens areas when the fringe density is not zero, which results in a retrace error at the zone lens itself, and additional retrace errors in the imaging optics of the interferometer.

Fig. 3 suggests at least two ways of determining the radius of the test sphere. When a DMI is available, it can be used to estimate the relative sphere positions that result in zero power for the inner and outer zone lenses, corresponding to the

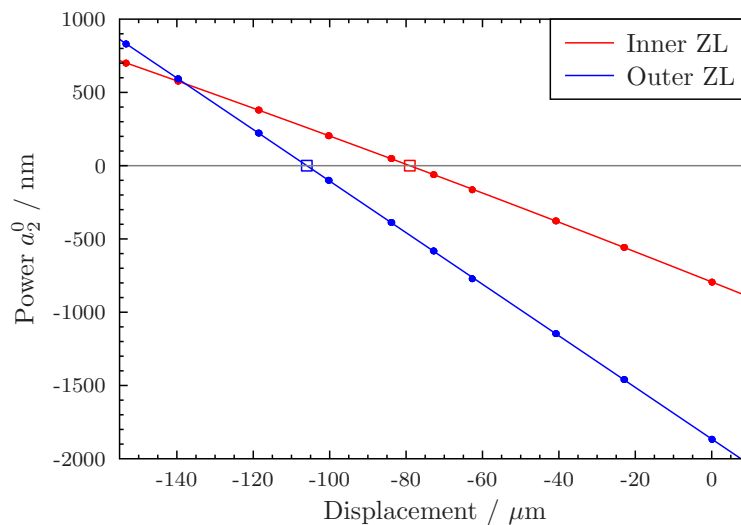


Figure 3. Defocus in the inner (blue) and outer (red) zone lenses as a function of displacement. A positive displacement moves the test sphere towards the nested zone lens. The curves are least-squares best-fit quadratic polynomials calculated from the measurement data.

zero crossings in Fig. 3. This approach is, in essence, identical to a radius bench measurement.<sup>2</sup> It incorporates accurate displacement measurements while avoiding the effects of non-zero fringe density and is thus likely to achieve the lowest measurement uncertainty. The radius  $R$  of the test part is calculated from the displacement  $z_o - z_i$  between the zero crossing  $z_o$  of the outer zone lens and  $z_i$  of the inner zone lens:

$$R = z_o - z_i + f_o - f_i, \quad (1)$$

where  $f_o$  is the primary focal length of outer zone lens and  $f_i$  the primary focal length of the inner zone lens. A positive displacement  $\Delta z$  moves the test part towards the zone lens. With design focal lengths of approximately 30 mm for the inner zone lens and approximately 110 mm for the outer zone lens, and the zero crossings calculated from the coefficients of a best-fit 2<sup>nd</sup> order polynomial as shown in Fig. 3, the resulting value for the radius  $R$  is 79988.306  $\mu\text{m}$ . This value deviates by 0.137  $\mu\text{m}$  from the reported radius of the test sphere.

An alternative way of using the nested zone lens is to measure the power term  $a_2^0$  in the outer zone lens area at the position of zero power in the inner zone lens. The advantage of this method is that a DMI system is no longer required. Its disadvantage is the need to make a measurement at non-zero fringe density in the outer zone lens area. Fig. 4 shows the power in the outer zone lens as a function of the power in the inner zone lens for the test part positions in Fig. 3. For our zone lens and test sphere, the power term  $a_2^0$  at zero power in the inner zone lens is -474.2 nm. The radius  $R$  of the test part can now be calculated using the following equation:

$$R = \Delta z_i - \Delta z_o + f_o - f_i = -\Delta z_o + f_o - f_i, \quad (2)$$

where  $\Delta z_o$  is the part displacement corresponding to the power  $a_2^0$  of the outer zone lens. For the outer zone lens the displacement can be approximated as:

$$\Delta z = -\alpha a_2^0, \quad (3)$$

where the dimensionless factor  $\alpha$  is given by:

$$1/\alpha = \frac{1}{4} \left( \frac{d_o}{2f_o} \right)^2 \left[ 1 - \frac{3}{4} \left( \frac{d_o}{2f_o} \right)^2 \right]. \quad (4)$$

$d_o$  is the diameter of the outer zone lens at the normalization image radius used to estimate  $a_2^0$ . Eqs. 3 and 4 represent a linear approximation of the non-linear relation between the defocus term  $a_2^0$  and part displacement  $\Delta z$ . The equation also incorporates an approximated correction for the effect on the estimated defocus term of the non-quadratic wavefront errors that occur when moving the test part. The errors introduced by both approximations increase for larger displacements from null. A more accurate estimate for the displacement  $\Delta z$  can be obtained by fitting the modeled wavefront error, parametrized in  $\Delta z$ , to the observed wavefront error.

For our outer zone lens with 60 mm diameter the displacement  $\Delta z$  is 27.016  $\mu\text{m}$ , which results in a radius  $R$  of 79988.248  $\mu\text{m}$ . This radius value deviates by 0.079  $\mu\text{m}$  from the actual radius of the test sphere. The weakness of this radius measurement method is evident from Eqs. 3 and 4. The uncertainty of the displacement  $\Delta z$  depends on the uncertainty of the power term  $a_2^0$ , which is *amplified* by a factor  $\alpha$ . In the case of our outer zone lens,  $\alpha \approx 57$ ; one nm of uncertainty in  $a_2^0$  is translated into an uncertainty of 57 nm in  $\Delta z$ , and thus  $R$ . For the inner zone lens the amplification factor  $\alpha$  is even larger; it equals 103.

Several important contributors to the measurement uncertainty must be considered, especially when measurements at non-zero fringe density are made to estimate the test sphere radius.

1. The XCALIBIR phase-shifting interferometer uses a single-frequency diode laser as its light source. The wavemeter that was used to measure the laser wavelength has a measurement uncertainty of approximately 1 pm. In addition, we found that the laser wavelength drifted by approximately 2 pm over the time of the measurements. This wavelength change causes a different change in the focal lengths of the zone lenses. The change  $\Delta f$  in the focal length  $f$  resulting from a change  $\Delta \lambda$  of the wavelength  $\lambda$  is:

$$\Delta f = -\frac{\Delta \lambda}{\lambda} \sqrt{f^2 + \left( \frac{d}{2} \right)^2}. \quad (5)$$

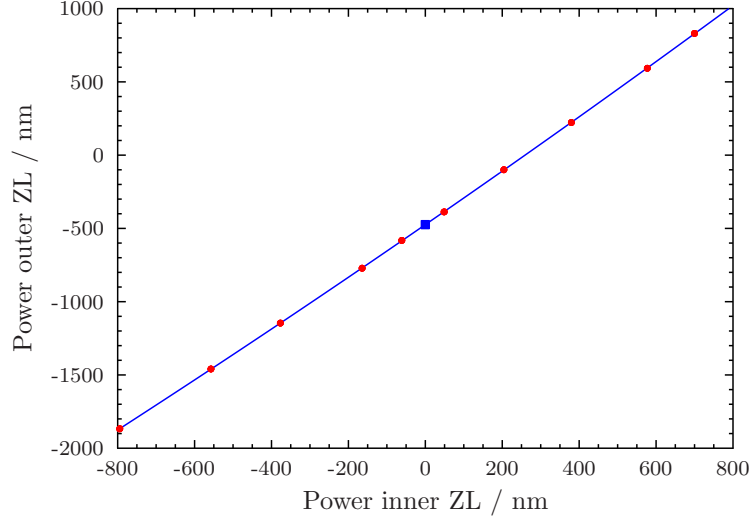


Figure 4. Measured power in the outer zone lens as function of the power in the inner zone lens (red data points) and a quadratic fit to the data (blue line). The power in the outer zone lens area at zero power in the inner zone lens area is -474.22 nm.

For the inner zone lens the focal length change corresponding to a wavelength change of 2 pm is  $-0.1 \mu\text{m}$ . The focal length of the outer zone lens changes by  $-0.36 \mu\text{m}$ . In our analysis we used the focal lengths corresponding to the average observed wavelength.

2. When a DMI system is used to determine the location of zero crossings in  $a_2^0$ , finding the precise locations of the zero crossings is complicated by the non-linear dependency of  $a_2^0$  on the test part displacement. In practice, the resulting error is minimized by performing several measurements in close proximity to null. In measurements without a DMI, either the inner or the outer zone lens must be measured at non-zero fringe density, which introduces errors in the estimated displacements  $\Delta z$  due to retrace errors and the linear approximation used to estimate  $\Delta z$  from  $a_2^0$  (Eqs. 3 and 4).
3. The uncertainty in the zone plate image normalization radius  $\rho_1$  (unit circle radius) that is used in the calculation of  $a_2^0$  has a significant effect on the uncertainty of the displacement  $\Delta z$  calculated with Eq. 3. The error  $E(\Delta z)$  caused by a relative error  $\Delta\rho_1/\rho_1$  in the image radius  $\rho_1$  can be approximated as:

$$E(\Delta z) = 2\Delta z \frac{\Delta\rho_1}{\rho_1} . \quad (6)$$

For our outer zone lens with  $\Delta z=27 \mu\text{m}$ , a relative error in the unit circle radius of  $\Delta\rho_1/\rho_1=10^{-3}$ , results in an error  $E(\Delta z)$  in the displacement  $\Delta z$  of 54 nm.

4. Fabrication errors of the Fresnel zone lenses, or thermal expansion of the substrate, affect the focal lengths of the zone lenses. For a zone lens with nominal diameter  $d$  that has a scale error  $\Delta d/d$ , the resulting error in the focal length can be approximated from the Fresnel zone lens equation. The resulting expression for  $\Delta f$  is:

$$\Delta f = \left( f + \sqrt{f^2 + (d/2)^2} \right) \frac{\Delta d}{d} . \quad (7)$$

The factor  $\Delta d/d$  can result from a scale error in the displacement metrology of the lithography tool that was used to fabricate the zone lens. A scale error can also occur when the zone lens is fabricated and used at different temperatures. For the outer zone lens with 110 mm focal length and 60 mm diameter, a scale error  $\Delta d/d = 10^{-6}$  results in a focal length error of  $\Delta f_o = 224 \text{ nm}$ . For the inner zone lens the respective error is 61 nm. The substrate material used for our zone lenses has a coefficient of thermal expansion (CTE) of  $3.25 \cdot 10^{-6}/\text{K}$ . The zone lenses were fabricated and used in laboratories that are temperature stabilized at  $(20 \pm 0.01) ^\circ\text{C}$ . A temperature mismatch of  $0.02 ^\circ\text{C}$  results in a radius error of about 11 nm.

5. A power component in the flatness error of the nested zone lens substrate results in an offset in the measured power of the inner and outer zone lenses because the unpatterned substrate surface is the reference surface of the interferometer cavity. The power component also results in a change in the focal lengths of the zone lenses. In our measurements the flatness error of the substrate was measured after zone lens fabrication and the flatness measurements were used to compensate the estimated radius for both effects.
6. When comparing two radius measurements, the form error of the test sphere can introduce bias when the measured test sphere area is not the same for both measurements. With our nested zone lens we measured the local radius of a relatively small area of the sphere, which can differ significantly from the best-fit radius of the whole sphere.<sup>3</sup>

Items 2 and 3 are the main reasons for the difference in the estimated radius between the two evaluated methods.

## 4. CONCLUSIONS

We have shown that nested Fresnel zone lenses can be used to measure the radius of precision surfaces with interferometry. The method has two advantages over the conventional radius bench method. First, it is possible to make radius measurements without a DMI system. The measurement uncertainty is larger in this case as when displacements can be measured with a DMI system, in particular for large radius errors due to the significant non-zero fringe densities. Lower uncertainties are achieved when the nested zone lens is combined with a DMI system. However, the uncertainty is still likely to be larger than that of a conventional radius bench because the zone lenses are much more sensitive to changes in laser wavelength and temperature than Fizeau objectives. The second, and perhaps most important, advantage of the nested zone lens method is that it extends the range of the radius bench method to spheres with large radii, because the length of the radius bench no longer needs to be at least as large as the test part radius. Our measurements of the radius of a precision sphere with a nominal radius of 80 mm agree surprisingly well with previous measurements, given that our measurements currently have a larger uncertainty.

## Acknowledgments

Zone lenses for our research were in part fabricated using facilities at the NanoFab of the NIST Center for Nanoscale Science and Technology. We are grateful to Taylor Hobson Ltd., UK, for the loan of a convex reference sphere.

## REFERENCES

- [1] van Brug, H., "Glass – Working optical applications," in [*Encyclopedia of Optical Engineering*], Driggers, R. G., ed., 667–674, Taylor & Francis (2007).
- [2] Selberg, L., "Radius measurement by interferometry," *Opt. Eng.* **31**, 1961–1966 (1992).
- [3] Griesmann, U., Soons, J., and Wang, Q., "Measuring form and radius of spheres with interferometry," *CIRP Ann.-Manuf. Technol.* **53**, 451–454 (2004).
- [4] Greivenkamp, J. E. and Bruning, J. H., "Phase shifting interferometry," in [*Optical Shop Testing, 2<sup>nd</sup> Edition*], Malacara, D., ed., 577–580, Wiley, New York (1992).
- [5] Schmitz, T. L., Davies, A. D., and Evans, C. J., "Uncertainties in interferometric measurements of radius of curvature," *Proc. SPIE* **4451**, 432–447 (2001).
- [6] Schmitz, T. L., Evans, C. J., Davies, A., and Estler, W. T., "Displacement uncertainty in interferometric radius measurements," *CIRP Ann.- Manuf. Technol.* **51**, 451–454 (2002).
- [7] Wang, Q., Gao, G., and Griesmann, U., "Radius measurement of spherical surfaces with large radii-of-curvature using dual-focus zone plates," in [*Optical Fabrication and Testing (OF&T)*], *OSA Technical Digest Series* (2008).
- [8] Chang, Y.-C. and Burge, J. H., "Error analysis for CGH optical testing," *Proc. SPIE* **3782**, 358–366 (1999).
- [9] de Groot, P., "Derivation of algorithms for phase-shifting interferometry using the concept of a data-sampling window," *Appl. Opt.* **34**, 4723–4730 (1995).
- [10] Menon, R., Patel, A., Chao, D., Walsh, M., and Smith, H. I., "Zone-Plate-Array Lithography (ZPAL): optical mask-less lithography for cost-effective patterning," *Proc. SPIE* **5751**, 330–339 (2005).
- [11] Smith, H. I., Walsh, M. E., Zhang, F., Ferrera, J., Hourihan, G., Smith, D., Light, R., and Jaspan, M., "An innovative tool for fabricating computer-generated holograms," *J. Phys.: Conf. Ser.* **415**, 012037 (2013).

- [12] Poleshchuk, A. G. and Nasyrov, R. K., "Aspheric wavefront shaping with combined computer generated holograms," *Opt. Eng.* **52**, 091709 (2013).
- [13] Malacara, D. and DeVore, S. L., "Interferogram evaluation and wavefront fitting," in [*Optical Shop Testing, 2<sup>nd</sup> Edition*], Malacara, D., ed., 455–499, Wiley, New York (1992).
- [14] Smith, W. J., "Modern optical engineering – 2<sup>nd</sup> edition," 328–329, McGraw-Hill, Boston (1990).